Article

A Multireference View of Photosynthesis: Uncovering Significant Site Energy Variations among Isolated Photosystem II Reaction Center Chlorophylls

Lea Northcote Sørensen,* Luca De Vico, and Thorsten Hansen*

Read Online

ACCESS | Metrics & More | Article Recommendations | SI Supporting Information

ABSTRACT: Oxygenic photosynthesis begins in the reaction center (RC) of the protein complex photosystem II (PSII). PSII has an intriguing, nearly symmetrical arrangement of cofactors within its RC. Despite this symmetry, evolution has favored only one of the two branches of PSII for efficient electron transfer. Current spectroscopic experiments explore the electronic dynamics during the picoseconds after energy has entered the RC and until the electron transfers to the pheophytin of the first branch. We present state-of-the-art multiconfigurational multireference calculations of the excitation energies or site energies of the four chlorophyll pigments of the RC without protein environment considerations. We see a significant variation that breaks the apparent symmetry of the RC. The inner chlorophyll of the productive RC branch possessed the lowest excitation energy of the four central chlorophylls. Our computational method used here is expensive; thus, geometry optimization of the crystal structure is currently not possible. In future work, charge and energy dynamics within the RC will be included as well as a dynamic description of the protein environment and its coupling to the RC. Other state-of-the-art studies of the RC, at lower levels of electronic structure, include a static treatment of the protein environment. These almost unanimously report that the outer chlorophyll of the active branch had the lowest excitation energy. Future work is needed to reconcile this discrepancy.

Photosystem II

δ+

Chl$_{D1}$ Chl$_{D2}$

P$_{D1}$ P$_{D2}$

SA-RASSCF/MS-RASPT2
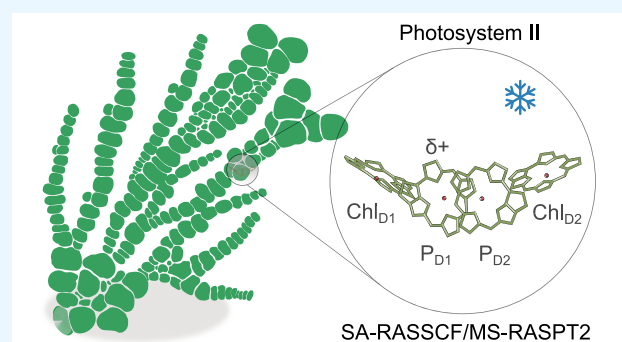
1. INTRODUCTION

Photosynthesis, the transfer of energy from sunlight to molecules, forms the basis of life on Earth. Solar excitation energy is captured by light-harvesting complexes in photosynthetic organisms and transferred to the reaction center (RC) within the energy-converting complex. In the RC, the excitation energy is converted into chemical energy with high quantum efficiency in the form of a charge-separated state.[1,2] From here, electron-transfer chains channel an electron out through the complex to other protein complexes, ultimately producing fuel molecules for the cell. Despite our knowledge of the pathways and time scales of the initial charge separation,[2] a detailed understanding of the mechanism responsible for the high efficiency of the process is missing.

The study of photosynthesis is motivated by the prospect of understanding its design principles. This knowledge can be used to design biomimetics which can be utilized in technologies such as solar fuel production and Power-to-X.[3] The fundamental question of this field is how the initializing excited states and the charge-transfer states lead to productive charge separation.[4,5]

Photosystem II (PSII) is the protein complex (Figure 1a) responsible for the light-driven oxidation of water into molecular oxygen and the supply of reducing agents in oxygenic photosynthesis.[2] The pigments of the RC (Figure 1b) are bound by protein chains D1 and D2, which are arranged in two nearly symmetrical branches. Each branch has a central chlorophyll a molecule called P$_{D1}$ and P$_{D2}$, respectively, a second chlorophyll molecule, Chl$_{D1}$ and Chl$_{D2}$, and a pheophytin molecule, Pheo$_{D1}$ and Pheo$_{D2}$, which together comprise the six core pigments of the PSII RC. Beyond these, a plastoquinone, Q$_A$ and Q$_B$, and a further peripheral chlorophyll, ChlZ$_{D1}$ and ChlZ$_{D2}$, are found on each chain.

The process of photosynthesis starts with the absorption of a photon by a light-absorbing pigment, which could be either in the inner light-harvesting complexes of PSII, CP43, and CP47 (Figure 1a) or in more peripheral light-harvesting complexes. The excitation energy hops from pigment to pigment and ends up at the RC. Here, a significant charge separation process takes place. Within 0.3−3.0 ps after the initial charge
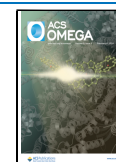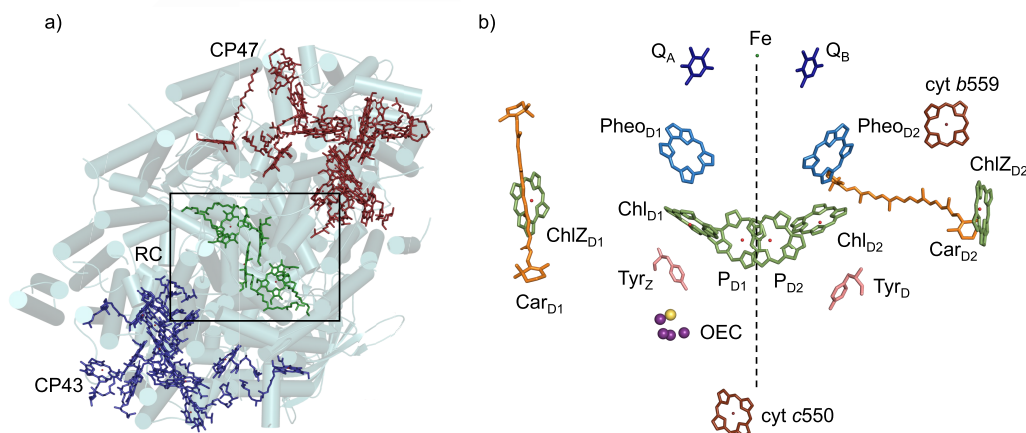
Figure 1. Elements of photosystem II (PSII). (a) Representation of one monomer of the PSII complex from *Thermostichus vulcanus* (PDB ID: 3WU2). The chlorophylls of the CP43 and CP47 subunits, as well as of the RC, are displayed. All chromophores are held in place by the protein matrix, which is mostly comprised of α-helices (cylinders). (b) Zoom-in of the RC where important structural components are shown. The dashed line illustrates the axis of pseudo-C2 symmetry.

separation, a radical pair species is formed with an estimated redox potential of 1.1−1.3 eV.[6−10]

A distinctive feature of PSII is the exclusive utilization of the D1 branch for electron transfer, following charge separation. The radical anion is localized on $Pheo_{D1}$[11−15] and the accompanying hole is mainly localized on P_{D1}.[16,17] The powerfully oxidizing cation of the radical pair, known as P680+, proceeds to abstract an electron from a water molecule, which is bound at the oxygen-evolving complex via a tyrosine residue, Tyr_Z. After four successive excitations and electron-transfer cycles, two water molecules are oxidized to form one oxygen molecule as a byproduct. Meanwhile, $Pheo_{D1}^-$ transfers an electron to plastoquinone Q_A, which in turn reduces the loosely bound plastoquinone Q_B. After a second successive excitation and electron-transfer cycle, Q_B^- is further reduced to Q_B^{2-} and becomes protonated to plastoquinol, Q_BH_2. Plastoquinol then leaves the binding site to carry its reducing equivalents to another protein complex, photosystem I, and is replaced by a new plastoquinone.[18,19]

Many groups have modeled this system. Most models of exciton dynamics in the literature build on fits to a series of spectroscopic experiments.[20−22] However, experimental excitation energies for individual chlorophyll monomers in the PSII complex are unavailable. Therefore, accurate calculation of the excited states and associated absorption spectrum of chlorophyll *a* molecules has long been a goal of quantum chemistry.[23−25] The site energies determine the trapping site of the excitation energy and the nature and directionality of the charge separation. Accurate site energies are, therefore, a critical requirement in order to understand the mechanism behind photosynthesis.

Time-dependent density functional theory (TD-DFT) has been used in several different variations,[26−34] as well as DFT/multireference configuration interaction (MRCI)[35] and various wave function methods, such as the symmetry adapted cluster/configuration interaction (SAC−CI),[30,36] second-order approximate coupled cluster singles and doubles model (CC2),[37] and the algebraic diagrammatic construction of second order [ADC(2)][37,38] to obtain excitation energies for chlorophyll *a*.

These studies preceded calculations based on PSII crystal structure coordinates.

Excitation energies of the RC sites, where the protein environment is included in the calculations, are available in the literature, and exciton dynamics studies based on these energetics exist.[39−43] The two most recent studies performed quantum mechanics/molecular mechanics (QM/MM) geometry optimizations on the crystal structure.[41,42] In QM/MM, the environment is included in the form of electrostatics. The choice of method, the assignment of the QM and MM regions, and the treatment of the atoms at the boundary between the regions must be considered when performing QM/MM. The two research groups that performed TD-DFT QM/MM on the system both found that Chl_{D1} had the lowest excitation energy of the four central chlorophylls.[41,42] They had differences in the order of the calculated chlorophyll excitation energies as well as in the absolute numbers, which can be attributed to differences in the methods of their calculations.

Tamura et al. used the CAM-B3LYP functional using the range-separation parameters, μ of 0.14, α of 0.19, and β of 0.46, whereas Sirohiwal et al. used the ωB97X-D3(BJ) functional along with the Def2-TZVP basis set. Sirohiwal et al. tested their TD-DFT method against a domain-based local pair natural orbital (DLPNO) implementation of the similarity transformed equation of motion coupled cluster theory with single and double excitations (STEOM-CCSD), which they had previously shown to be accurate in calculating the absorption spectrum of chlorophyll *a*, except a red shift in the values.[44] For geometry optimization, Tamura et al. used B3LYP and Sirohiwal et al. used PBE. Later, Sirohiwal et al. performed a study showing that the range-separated functionals, including the ωB97 functional, but outperformed by ωB2PLYP, correctly reproduced the energy shifts of the RC from PSII, whereas CAM-B3LYP underestimated the shifts.[45]

Recently, Cignoni et al. published a study using machine learning to predict excitonic couplings for light-harvesting complexes,[46] which they later extended to estimate site energies.[47] They tested their method against the M062X/6-31G(d) level of theory TD-DFT QM/MM data and showed good agreement with data outside their training set. However,

they did not test it against higher-level methods. Using machine learning to obtain parameters for strongly conjugated systems could provide a quick way to acquire numbers comparable to those of TD-DFT QM/MM methods.

In the current study, we apply a multiconfigurational multireference method that we previously applied to bacteriochlorophyll units in LH2 and LH3[48,49] to calculate the excitation energies of the four central chlorophylls of the PSII RC. We present the site energies and transition dipole moments (TDMs) obtained from state-average restricted active space self-consistent field (SA-RASSCF)/multistate second-order perturbation theory (MS-RASPT2) calculations. These values provide a detailed view into the vacuum energetics of the RC of PSII and can be used in future dynamics simulations of ultrafast spectroscopy of PSII.

The geometries used to calculate the excitation energies are taken directly from the 1.9 Å crystal structure.[50] No geometry optimization is performed, as this is out of reach for the electronic structure used.

Our calculations do not involve the protein environment in any way other than the spatial positioning of the heavy atoms. We provide vacuum numbers for the site energies for use in quantum dynamical simulations. Excluding the protein environment in the site energies ensures that no double-counting effects occur when a model for the environment is explicitly applied in the simulations. These highly accurate vacuum excitation energies are the first step in obtaining new insights into the mechanism behind photosynthesis.

2. RESULTS AND DISCUSSION

2.1. Wave Function Analysis. SA-RASSCF/MS-RASPT2 calculations require high costs in terms of computational resources. To justify the need for multiconfigurational calculations, we provide here an analysis of the wave function obtained for chlorophyll *a*. Table 1 reports the wave function components for the ground and first excited state of P_{D2} with CI coefficients larger than 0.05. Raw data are reported in Table S5 in the Supporting Information.

The ground-state wave function is constituted by around 65% of the SCF ground-state configuration, by single excitation configurations for at least 0.4% and by double excitation configurations for at least 4.9%. The remaining 30% is attributed to configurations with CI coefficients of less than 0.05. The first excited-state wave function is constituted of single excitations for at least 61%, double excitations for at least 4.8%, and triple excitation configurations for at least 0.7%. Again, the remaining 34% is due to configurations with CI coefficients smaller than 0.05.

The wave function composition of chlorophyll *a* follows the trend from our study on bacteriochlorophyll *a*[48] and is in agreement with previous findings for chlorophyll *a* from a DFT/MRCI investigation.[35] However, the percentages of the single excitations in the DFT/MRCI calculations were higher than what we found in this study, and no contribution from triple excitations for the first excited state was reported in the other study. The SCF weight of the ground-state configuration, $C_0^2 < 0.90$, together with the partial electronic occupation of the AS orbitals (Table S5 in the Supporting Information) arbitrate the need for a multiconfigurational treatment. Figure 2 solidifies that the nature of the excitation involves all four orbitals in RAS2.

2.2. Ground-State Energies. Table 2 presents the computed ground-state energies relative to the lowest

Table 1. Wave Function Components for P_{D2} of the Ground and First Excited State after MS-RASPT2 Single-Point Energy Evaluation[a]

type	configuration	percentage (%)
	ground state	
G	SCF ground state	64.9
D	$\pi_{RAS2}^2 \to \pi_{RAS2}^2$	3.4
D	$\pi_{RAS1}^1 \pi_{RAS2}^1 \to \pi_{RAS2}^1 \pi_{RAS2}^1$	2.5
D	$\pi_{RAS1}^1 \pi_{RAS2}^1 \to \pi_{RAS2}^1 \pi_{RAS3}^1$	1.0
S	$\pi_{RAS1}^1 \to \pi_{RAS2}^1$	0.4
D	$\pi_{RAS1}^2 \to \pi_{RAS3}^1 \pi_{RAS3}^1$	0.3
	first excited state	
S	$\pi_{RAS2}^2 \to \pi_{RAS2}^1$	60.8
D	$\pi_{RAS1}^1 \pi_{RAS2}^1 \to \pi_{RAS2}^1 \pi_{RAS2}^1$	1.5
D	$\pi_{RAS2}^2 \to \pi_{RAS2}^1 \pi_{RAS3}^1$	1.1
D	$\pi_{RAS2}^1 \pi_{RAS2}^1 \to \pi_{RAS2}^1 \pi_{RAS3}^1$	0.8
T	$\pi_{RAS2}^1 \pi_{RAS2}^2 \to \pi_{RAS2}^2 \pi_{RAS2}^1$	0.7
G	SCF ground state	0.5
S	$\pi_{RAS1}^1 \to \pi_{RAS2}^1$	0.4
D	$\pi_{RAS1}^2 \to \pi_{RAS2}^1 \pi_{RAS3}^1$	0.4
S	$\pi_{RAS1}^1 \to \pi_{RAS3}^1$	0.4
D	$\pi_{RAS1}^1 \pi_{RAS2}^1 \to \pi_{RAS2}^2$	0.7
D	$\pi_{RAS2}^1 \pi_{RAS2}^1 \to \pi_{RAS2}^1 \pi_{RAS2}^1$	0.3

[a]Ground state (G), single (S), double (D), and triple (T) excitation. In the SCF ground state, all of the RAS1 orbitals are fully occupied as well as two of the four RAS2 orbitals. The notation, e.g., $\pi_{RAS1}^1 \pi_{RAS2}^1 \to \pi_{RAS2}^{22}$ indicates a configuration where one electron from a π-orbital in RAS1 and one electron from a π-orbital in RAS2 were both excited to a π-orbital in RAS2 (empty in the SCF ground state). Only configurations with a CI coefficient larger than 0.05 are included.

Occ. root 1: 1.852
Occ. root 2: 1.713
Average occ.: 1.778

Occ. root 1: 1.824
Occ. root 2: 1.169
Average occ.: 1.504

Occ. root 1: 0.202
Occ. root 2: 0.850
Average occ.: 0.529

Occ. root 1: 0.148
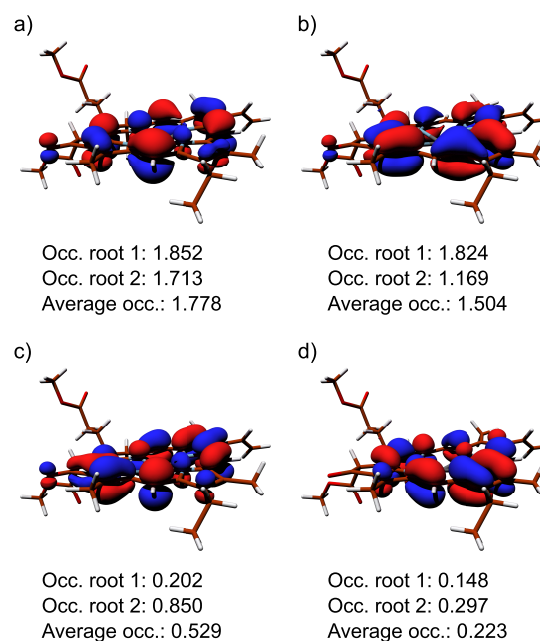Occ. root 2: 0.297
Average occ.: 0.223

Figure 2. Representation of the orbitals included in the RAS2 space for the chlorophyll *a* unit. For each orbital, the electron occupation is given for the ground (root 1) and excited (root 2) states as well as their average. (a, b) are the highest-lying orbitals where excitation can occur. (c, d) are the lowest-lying orbitals to which excitation can occur. It is possible to see that the electronic excitation involves mainly (b, c), although it is not only limited to these two orbitals.

Table 2. MS-RASPT2 Ground-State Relative Energies of PSII RC Sites[a]

site	relative energy	
	(kcal/mol)	(eV)
P_{D1}	0.48	0.02
P_{D2}	10.64	0.46
Chl_{D1}	0.00	0.00
Chl_{D2}	0.33	0.01

[a]The values are relative to the lowest ground-state energy, Chl_{D1}. Absolute energies are given in Table S6 in the Supporting Information.

ground-state energy of the four chlorophyll units, while absolute energies are given in Table S6 in the Supporting Information. The two outer chlorophylls have ground-state energies lower than those of the inner chlorophylls. Chl_{D1} has the lowest ground-state energy. P_{D2} stands out with a relative energy of 0.46 eV compared to Chl_{D1}. This means that energetically, the symmetry is slightly broken. The relative difference between the most extreme values, P_{D2} and Chl_{D1}, equals almost 18 times the room temperature thermal energy, hence it is expected to be significant even after thermal averaging.[51]

Scrutinizing the geometries of the four chlorophylls, a twisting of the side double bond adjacent to the ring is observed for P_{D2}, which can explain the higher ground-state energy of this unit compared with the others. In Figure 3, α marks the single bond around which the double bond can twist. When the double bond is in a conformation out of the π-system plane, it overlaps less with the rest of the π-system and
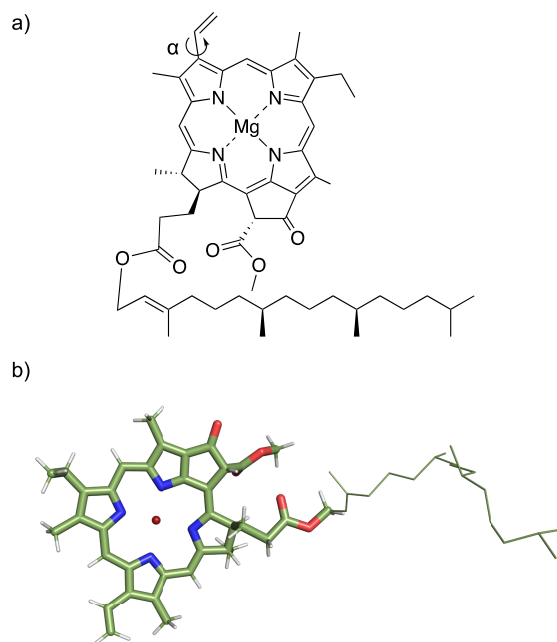

Figure 3. Structure of the chlorophyll units. (a) Line-drawing structure of chlorophyll *a*. (b) One of the chlorophyll *a* units extracted from the crystal structure. Hydrogen atoms were added to the heavy-atom crystal coordinates, and the phytyl tail (lines) was removed and substituted with a methyl group.

therefore gives a smaller degree of π-conjugation to the unit (destabilization), which, in turn, increases the ground-state energy.

2.3. Excited-State Energies. Table 3 reports the computed excitation energies of the four central chlorophylls

Table 3. Excitation Energies and Oscillator Strengths of RC Sites in PSII Computed with MS-RASPT2[a]

chlorophyll	excitation energy		oscillator strength
	(eV)	(cm^{-1})	
P_{D1}	2.059	16,605	0.2082
P_{D2}	2.085	16,818	0.2511
Chl_{D1}	2.101	16,945	0.2282
Chl_{D2}	2.160	17,421	0.1494

[a]Absolute energies are reported in Table S6 in the Supporting Information.

along with the respective oscillator strengths. P_{D1} has the lowest excitation energy followed by P_{D2}. Chl_{D2} has the highest excitation energy of the four sites. The oscillator strength is highest for P_{D2} followed by Chl_{D1}, and then P_{D1} comes before Chl_{D2}, which has a significantly smaller oscillator strength compared to those of the other chlorophylls. The twisting of the double bond attached via α in Figure 3 appears to not affect the excited state in the same way as the ground state. P_{D2} has a lower excitation energy compared to the two outer chlorophylls, even though its ground-state energy was elevated. The excitation energies of the D1 side chlorophylls are both lower than their D2 counterparts, which further supports the idea of asymmetry in the RC.

Lots of values for the site energies in the PSII RC are available in the literature, see Table 4. Before 2014, all literature excitation energy values for the four chlorophylls of the PSII RC came from experimental parameter fits. In the experimental studies, a fitting procedure is performed on spectroscopic data of reduced versions of the protein complex. When spectroscopic measurements are performed, the surrounding protein and possibly solvent can affect the measurements and, thereby, the obtained excitation energies.

In the first model from 1995, the chlorophylls had equal excitation energies.[61] In 2000, Prokhorenko and Holzwarth suggested that Chl_{D1} had a slightly higher excitation energy than the other chlorophylls in the RC.[60] Two papers from 2002 went back to the multimer model where all four chlorophylls have the same excitation energy.[58,59] From 2005 onward, only models with differences in excitation energies were presented.[14,39,40,42,52−57,62,63] The only partial exception is represented by model C of the 2005 Novoderezhkin et al. paper, where the outer chlorophylls have the same excitation energy.[57] Chl_{D1} is reported to have the smallest excitation energy in all studies, except for the 2011 paper by Novoderezhkin et al., where Chl_{D2} is reported to have the lowest excitation energy.

In 2014, the first computational study of the excitation energies of the RC of PSII was published. Zhang et al. employed a combination of extensive molecular dynamics (MD) simulations with ZINDO/S QM/MM calculations based on the crystal structure of PSII to compute site energies.[39] This study found excitation energies lower than those previously reported. They saw a higher variation when they increased the temperature during the MD simulation. They did not see variation among site energies when they

Table 4. Transition Energies of the Four Central Chlorophylls Compared to the Literature Values in Chronological Order[a]

	excitation energy (eV)				relative variation (eV)[b]			
dataset	P_{D1}	P_{D2}	Chl_{D1}	Chl_{D2}	P_{D1}	P_{D2}	Chl_{D1}	Chl_{D2}
Current study	**2.059**	**2.085**	**2.101**	**2.160**	**0.000**	**0.026**	**0.042**	**0.101**
Sirohiwal et al. 2020[42]	**1.925**	**1.927**	**1.920**	**1.943**	**0.005**	**0.007**	**0.000**	**0.023**
<u>Sirohiwal et al. 2020[42]</u>	<u>1.907</u>	<u>1.904</u>	<u>1.856</u>	<u>1.916</u>	<u>0.051</u>	<u>0.048</u>	<u>0.000</u>	<u>0.060</u>
<u>Tamura et al. 2020[41]</u>	<u>2.064</u>	<u>2.088</u>	<u>2.012</u>	<u>2.041</u>	<u>0.052</u>	<u>0.076</u>	<u>0.000</u>	<u>0.029</u>
<u>Müh et al. 2017[40]</u>	<u>1.855</u>	<u>1.855</u>	<u>1.827</u>	<u>1.849</u>	<u>0.028</u>	<u>0.028</u>	<u>0.000</u>	<u>0.022</u>
<u>Zhang et al. 2014 77K[39]</u>	<u>1.605</u>	<u>1.613</u>	<u>1.586</u>	<u>1.625</u>	<u>0.019</u>	<u>0.027</u>	<u>0.000</u>	<u>0.039</u>
<u>Zhang et al. 2014 300K[52]</u>	<u>1.593</u>	<u>1.598</u>	<u>1.566</u>	<u>1.590</u>	<u>0.027</u>	<u>0.032</u>	<u>0.000</u>	<u>0.024</u>
Shibata et al. 2013[53]	1.866	1.853	1.827	1.858	0.039	0.026	0.000	0.031
Gelzinis et al. 2013[52]	1.893	1.885	1.861	1.873	0.032	0.024	0.000	0.012
Novoderezhkin et al. 2011[54]	1.891	1.882	1.871	1.862	0.029	0.020	0.009	0.000
Raszewski and Renger 2008 >170K[14]	1.860	1.860	1.817	1.858	0.043	0.043	0.000	0.041
Novoderezhkin et al. 2007[55]	1.882	1.881	1.859	1.875	0.023	0.022	0.000	0.016
Raszewski and Renger 2005[56]	1.885	1.885	1.852	1.882	0.033	0.033	0.000	0.030
Novoderezhkin et al. 2005 A[57]	1.874	1.880	1.872	1.872	0.002	0.008	0.000	0.000
Novoderezhkin et al. 2005 B[57]	1.872	1.912	1.869	1.900	0.003	0.043	0.000	0.031
Novoderezhkin et al. 2005 C[57]	1.886	1.886	1.860	1.889	0.026	0.026	0.000	0.029
Novoderezhkin et al. 2005 D[57]	1.894	1.872	1.863	1.874	0.031	0.009	0.000	0.011
Renger and Marcus 2002[58]	*1.852*	*1.852*	*1.852*	*1.852*	*0.000*	*0.000*	*0.000*	*0.000*
Jankowiak et al. 2002[59]	*1.841*	*1.841*	*1.841*	*1.841*	*0.000*	*0.000*	*0.000*	*0.000*
Prokhorenko and Holzwarth 2000[60]	*1.841*	*1.841*	*1.846*	*1.841*	*0.000*	*0.000*	*0.005*	*0.000*
Durrant et al. 1995[61]	*1.841*	*1.841*	*1.841*	*1.841*	*0.000*	*0.000*	*0.000*	*0.000*

[a]Computational studies are marked with an underline. The bold entries are computational studies performed in vacuum. Italicized entries are multimer models with identical excitation energies. [b]Relative variation compared to the lowest excitation energy for each study.

performed the ZINDO/S calculation in a vacuum on geometries from the crystal structure. A relaxation of the crystal structure by extensive MD simulations was necessary to see the site energy variations.

In 2017, Müh et al. applied a quantum-chemical computational method based on a numerical solution of the linearized Poisson−Boltzmann equation, denoted PBQC, on the RC of PSII.[40] They performed the PBQC method directly on the crystal structure coordinates and found site energy variations comparable to Zhang et al.'s MD results.

The two research groups that performed TD-DFT QM/MM studies of the system in 2020 both found larger variations among the sites than the previous studies.[41,42] Both groups found that the inclusion of the protein environment in the QM/MM calculation decreased the excitation energy for Chl_{D1} to a larger extent than the other site energies. Sirohiwal et al. performed an MD simulation where the protein was represented prior to QM/MM calculations. They performed vacuum QM/MM calculations and saw a much smaller variation between the sites.

Our variations between the site energies are in the same order as or higher than the thermal energy. Our highest variation is for Chl_{D2}, where the excitation energy relative to P_{D1} is 101 meV, which is equivalent to about 4 times the room temperature thermal energy ($k_B T \approx 26$ meV).[64]

The absence of geometry optimization in the presence of the protein environment explains the differences in our results compared with QM/MM studies in the literature. In the current study, we wished to separate the environmental effects from the excitation energies to provide parameters for a system Hamiltonian, where the environment can be applied subsequently in the quantum dynamics simulation. Our site energies indicate that the directionality of the charge separation process is finely tuned by the environment. Therefore, we need to treat it carefully.

We have chosen not to perform MD simulations or QM/MM optimizations prior to property calculation. Geometries from the same crystal structure give site energy differences that are on the same order of magnitude with or without geometry optimization. This has been shown in a study of LH2 by Cardoso Ramos et al.,[65] see Table S9 in the Supporting Information. A QM/MM geometry optimization prior to a SA-RASSCF/MS-RASPT2 single-point energy evaluation is in the works of our group, but we expect that our differences in site energies will be qualitatively maintained according to the results by Cardoso Ramos et al.

All previous studies report significantly lower excitation energies than the current study, except for the study by Tamura et al. where some of the site energies are higher than ours.[41] Performing geometry optimizations in the presence of a protein environment, in general, lowers excitation energies, so we expected to obtain higher excitation energies.

Another contribution to the high excitation energies could be that the MS-RASPT2 calculations include a zeroth-order Hamiltonian correction called the IPEA shift, which was designed to eliminate an underestimation in the energies of open-shell states that was observed in the calculation of dissociation energies in CASPT2 excitation energies. The correction has previously been shown to overestimate excitation energies with 0.1−0.5 eV.[66−69]

We performed the MS-RASPT2 calculations without IPEA shifts. The results can be seen in Table S10 in the Supporting Information. The differences to our calculations, including IPEA shifts, are between 0.27 and 0.30 eV and give excitation energies that are slightly lower than previously reported in the literature. The order of the site energies follows the trend we see when the IPEA shift is included in the calculations. We do not believe there is advocacy for using MS-RASPT2 values without IPEA shifts, and we, therefore, present our results with the standard IPEA shift.

2.4. TDM Vectors. Figure 4 shows the four central chlorophyll units together with their computed TDM vectors. The TDM vector components are given in Table S7 in the Supporting Information.
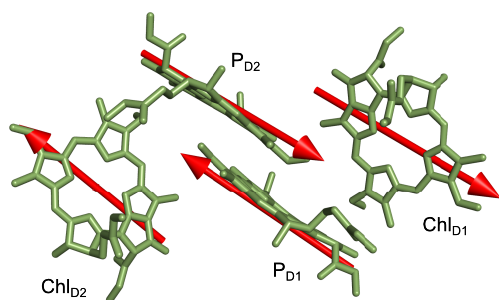

Figure 4. Representation of the computed TDM vectors of the four central chlorophylls. The vectors were drawn centered on the magnesium atom of each chlorophyll unit. The vector sizes were adjusted for clarity.

The TDMs follow the spatial disposition of the chlorophyll units. The direction of TDMs is opposite for the units that overlap in space. Hence, P_{D1} has a TDM going in the opposite direction of that of P_{D2} and Chl_{D1}, but Chl_{D2} has a TDM in the same direction as P_{D1}. Furthermore, there is a difference in the angles between the vectors of the two antiparallel TDMs.

Table 5 shows the angles between the various TDM vectors obtained as dot products. Even though it is a crude

Table 5. Angles between the Computed TDM Vectors Obtained from the Vector Dot Products[a]

site	P_{D1}	P_{D2}	Chl_{D1}	Chl_{D2}
P_{D1}		145.1	150.7	9.1
P_{D2}			5.7	137.6
Chl_{D1}				143.3
Chl_{D2}				

[a]The lower triangle is the mirror image of the upper and is omitted for clarity.

approximation, the angles between the TDMs can be interpreted as an indication that the coupling between P_{D1} and Chl_{D2} and between P_{D2} and Chl_{D1} is lower than all other combinations of couplings.

Additionally, the asymmetry of the angles in Table 5 gives further support to the hypothesis of asymmetry in the RC of PSII. However, the couplings between the chlorophyll units should be evaluated with higher precision methods for use in quantum dynamical simulations of the RC, which we are currently working on.

3. CONCLUSIONS

In the presented study, we used the multiconfigurational multireference SA-RASSCF/MS-RASPT2 method to compute excitation energies and corresponding TDMs of the four central chlorophylls of PSII. To the best of our knowledge, this is the first multireference report for chlorophyll *a* that, due to its highly conjugated nature, necessitates such a computationally costly treatment.

In the current study, we find that P_{D1} has the lowest excitation energy, followed by P_{D2} and Chl_{D1}. This is in opposition to the consensus in the literature that Chl_{D1} has the lowest excitation energy and that P_{D1} and P_{D2} have the highest energies. Our vacuum excitation energies are larger than the previous values in the literature because we exclude the protein environment in our calculations. The only exception in the literature is a TD-DFT QM/MM study by Tamura et al., where similar absolute values are obtained.[41]

We did not perform geometry optimization prior to the site energy calculation in this study. The goal of our study was to produce raw site energies without including the protein environment in the calculations. Based on the findings of Cardoso Ramos et al.,[65] where geometry optimization did not impact the trend nor the size of the site variation in LH2, we do not expect geometry optimizations to affect our observations.

Our results can be used for simulations of the quantum dynamics of the system. This could be simulations of ultrafast spectroscopies, which in conjunction with existing experimental data could illuminate the mechanism behind the charge separation process. Experimental data for the system are already available, and the urge to move forward in the field is here. Simulations of the system would require precise couplings in addition to the excitation energies, as these can substantially change the system dynamics. Because we present the raw numbers for the excitation energies, it is possible to treat the environment separately in quantum dynamics simulations.

We are currently working on computing the energetics of surrounding cofactors in the RC of PSII. Application of the SA-RASSCF/MS-RASPT2 method to other photoactive molecules and systems is a possibility in the future.

4. COMPUTATIONAL DETAILS

4.1. Structure Preparation. In this study, we employed coordinates of the four central chlorophylls from the 1.9 Å resolution dimeric crystal structure of PSII from *Thermostichus vulcanus*, PDB entry 3WU2,[50] as input for our calculations. The protein structure consists of two monomers each having an RC. We extracted the Cartesian coordinates of the four central chlorophyll *a* molecules from the first monomer in the PDB file. The saturated phytyl tails of the chlorophyll units were replaced by a methyl group, and hydrogen atoms were added to obtain the employed structure of the molecule; see Figure 3 and Tables S1−S4 in the Supporting Information. Because the coordinates from the crystal structure include the protein matrix-induced average geometrical distortion, we consider them to be a good representation of the RC structure. The protein environment around the four central chlorophylls was completely excluded from our calculations in order to provide raw numbers for the site energies.

4.2. Energy Evaluation. We performed single-point energy calculations at the SA-RASSCF/MS-RASPT2 level of theory. All calculations were performed on neutral molecules in vacuum.

For each chlorophyll unit, we computed two-root SA-RASSCF single-point energies. The RASSCF method is a more general extension of the complete active space self-consistent field (CASSCF)[70] method. They are both multiconfigurational methods, where the wave function is constructed as a linear combination of configuration state functions (CSFs). The number and type of available functions are determined by the

active space (AS) and the overall spin. In the case of chlorophyll *a*, the spin is a singlet state. In RASSCF, the AS orbitals are divided into three parts, namely, RAS1−3. The CSFs are built by distributing the active electrons into the active orbitals, following the rules of each RAS while maintaining the overall spin. The orbitals included in RAS2 can have any occupation. The orbitals in RAS1 are fully occupied in all CSFs, except for a specified number of possible vacancies, and likewise, the orbitals in RAS3 are empty, except for the same number of excitations.

In the study presented here, all π-orbitals of the conjugated system are included in the AS because the electronic excitations of chlorophyll *a* are dominated by $\pi-\pi^*$ transitions. Including the carbonyl π-orbitals in the AS allows for the evaluation of the different torsions of the moiety and the corresponding participation to the overall chlorophyll π-system. The AS choice is based on our previous investigation of the AS of bacteriochlorophylls,[48] which included four orbitals in RAS2 and had single, double, and triple excitations. However, because chlorophyll *a* has a slightly larger conjugated system than bacteriochlorophyll, 12 orbitals are included in RAS1 and 11 orbitals in RAS3, corresponding to the number of π-orbitals seen in Table S8 in the Supporting Information. This exceeds the AS from our previous study[48] which was one orbital smaller in both RAS1 and RAS3, with the current total number of active orbitals being 27 with 28 active electrons, compared to 25 orbitals with 26 electrons. This AS requires over 17 million CSFs which we evaluate to be at the top limit of the method, given the current hardware and a reasonable computational time (<3 weeks). All calculations employed an ANO-RCC basis set[71] with a double-ζ quality. The convergence thresholds for the SA-RASSCF calculations were set to 0.0001 for the energy, 0.1 for the orbital rotation matrix, and 0.0005 for the energy gradient. After a preliminary SCF calculation, the 1s orbitals of all non-hydrogen atoms, as well as the 2s and 2p orbitals of magnesium, were frozen in all following calculations.

The computed SA-RASSCF wave functions were used as reference configurations for subsequent MS-RASPT2 calculations. RASPT2 is an extension of the second-order perturbation theory method CASPT2 applied to a RASSCF-type reference wave function.[72] MS-RASPT2 is the corresponding multistate treatment similar to MS-CASPT2. MS-RASPT2 has been shown to output excitation energies equivalently good as MS-CASPT2 for different organic compounds.[73] To reduce the computational costs of the MS-RASPT2 calculations, 300 virtual orbitals were deleted. All MS-RASPT2 calculations employed an imaginary shift value of 0.1[74] and a standard IPEA shift,[75] except for the values in Table S10 in the Supporting Information where the IPEA shift was omitted.

All SA-RASSCF/MS-RASPT2 calculations were performed using OpenMolcas version 23.02.[76] The MS-RASPT2 calculations were split into two separate jobs running on different CPUs to accelerate the process. Preliminary hydrogen optimization was performed at the PM6[77] level of theory using the Gaussian16 suite.[78]

The calculations were performed on a dual processor (Intel Xeon Gold 6334 3.6G Dual CPU 1.6TB NVMe) and employed 200 GB of memory. Using the split and farming technique,[79] each MS-RASPT2 state energy calculation required, on average, 19 days.

■ ASSOCIATED CONTENT

Ⓢ Supporting Information

The Supporting Information is available free of charge at https://pubs.acs.org/doi/10.1021/acsomega.3c05331.

> Coordinates of chemical structures, wave function composition raw data, absolute energies, TDM vector components, and AS orbital depictions (PDF)

■ AUTHOR INFORMATION

Corresponding Authors

Lea Northcote Sørensen − *Department of Chemistry, University of Copenhagen, DK-2100 Copenhagen O, Denmark;* ⓞ orcid.org/0000-0002-4256-1856; Phone: +45 23 35 20 57; Email: l.northcote@chem.ku.dk

Thorsten Hansen − *Department of Chemistry, University of Copenhagen, DK-2100 Copenhagen O, Denmark;* ⓞ orcid.org/0000-0003-1813-5125; Phone: +45 22 29 57 28; Email: thorsten@chem.ku.dk

Author

Luca De Vico − *Department of Biotechnology, Chemistry, and Pharmacy, University of Siena, I-53100 Siena, Italy;* ⓞ orcid.org/0000-0002-2821-5711

Complete contact information is available at: https://pubs.acs.org/10.1021/acsomega.3c05331

Notes

The authors declare no competing financial interest.

■ REFERENCES

(1) Cheng, Y. C.; Fleming, G. R. Dynamics of light harvesting in photosynthesis. *Annu. Rev. Phys. Chem.* **2009**, *60*, 241−262.

(2) Blankenship, R. E. *Molecular Mechanisms of Photosynthesis*, 2nd ed.; Wiley-Blackwell, 2014.

(3) Lund, P. D.; Lindgren, J.; Mikkola, J.; Salpakari, J. Review of energy system flexibility measures to enable high levels of variable renewable electricity. *Renewable Sustainable Energy Rev.* **2015**, *45*, 785−807.

(4) Mamedov, M.; Govindjee; Nadtochenko, V.; Semenov, A. Primary electron transfer processes in photosynthetic reaction centers from oxygenic organisms. *Photosynth. Res.* **2015**, *125*, 51−63.

(5) Reimers, J. R.; et al. Challenges facing an understanding of the nature of low-energy excited states in photosynthesis. *Biochim. Biophys. Acta, Bioenerg.* **2016**, *1857*, 1627−1640.

(6) Rappaport, F.; Guergova-Kuras, M.; Nixon, P. J.; Diner, B. A.; Lavergne, J. Kinetics and pathways of charge recombination in photosystem II. *Biochemistry* **2002**, *41*, 8518−8527.

(7) Grabolle, M.; Dau, H. Energetics of primary and secondary electron transfer in photosystem II membrane particles of spinach revisited on basis of recombination-fluorescence measurements. *Biochim. Biophys. Acta, Bioenerg.* **2005**, *1708*, 209−218.

(8) Ishikita, H.; Saenger, W.; Biesiadka, J.; Loll, B.; Knapp, E. W. How photosynthetic reaction centers control oxidation power in chlorophyll pairs P680, P700, and P870. *Proc. Natl. Acad. Sci. U.S.A.* **2006**, *103*, 9855−9860.

(9) Kato, Y.; Sugiura, M.; Oda, A.; Watanabe, T. Spectroelectrochemical determination of the redox potential of pheophytin a, the

primary electron acceptor in photosystem II. *Proc. Natl. Acad. Sci. U.S.A.* **2009**, *106*, 17365−17370.

(10) Allakhverdiev, S. I.; Tomo, T.; Shimada, Y.; Kindo, H.; Nagao, R.; Klimov, V. V.; Mimuro, M. Redox potential of pheophytin a in photosystem II of two cyanobacteria having the different special pair chlorophylls. *Proc. Natl. Acad. Sci. U.S.A.* **2010**, *107*, 3924−3929.

(11) Dekker, J. P.; Van Grondelle, R. Primary charge separation in photosystem II. *Photosynth. Res.* **2000**, *63*, 195−208.

(12) Holzwarth, A. R.; Müller, M. G.; Reus, M.; Nowaczyk, M.; Sander, J.; Rögner, M. Kinetics and mechanism of electron transfer in intact photosystem II and in the isolated reaction center: pheophytin is the primary electron acceptor. *Proc. Natl. Acad. Sci. U.S.A.* **2006**, *103*, 6895−6900.

(13) Rutherford, A. W.; Osyczka, A.; Rappaport, F. Back-reactions, short-circuits, leaks and other energy wasteful reactions in biological electron transfer: redox tuning to survive life in O(2). *FEBS Lett.* **2012**, *586*, 603−616.

(14) Raszewski, G.; Renger, T. Light harvesting in photosystem II core complexes is limited by the transfer to the trap: can the core complex turn into a photoprotective mode? *J. Am. Chem. Soc.* **2008**, *130*, 4431−4446.

(15) Renger, T.; Schlodder, E. Optical properties, excitation energy and primary charge transfer in photosystem II: theory meets experiment. *J. Photochem. Photobiol., B* **2011**, *104*, 126−141.

(16) Saito, K.; Ishida, T.; Sugiura, M.; Kawakami, K.; Umena, Y.; Kamiya, N.; Shen, J. R.; Ishikita, H. Distribution of the cationic state over the chlorophyll pair of the photosystem II reaction center. *J. Am. Chem. Soc.* **2011**, *133*, 14379−14388.

(17) Narzi, D.; Bovi, D.; De Gaetano, P.; Guidoni, L. Dynamics of the special pair of chlorophylls of photosystem II. *J. Am. Chem. Soc.* **2016**, *138*, 257−264.

(18) Kavanagh, M. A.; Karlsson, J. K. G.; Colburn, J. D.; Barter, L. M. C.; Gould, I. R. A TDDFT investigation of the photosystem II reaction center: insights into the precursors to charge separation. *Proc. Natl. Acad. Sci. U.S.A.* **2020**, *117*, 19705−19712.

(19) Müh, F.; Glöckner, C.; Hellmich, J.; Zouni, A. Light-induced quinone reduction in photosystem II. *Biochim. Biophys. Acta, Bioenerg.* **2012**, *1817*, 44−65.

(20) Lewis, K. L.; Ogilvie, J. P. Probing photosynthetic energy and charge transfer with two-dimensional electronic spectroscopy. *J. Phys. Chem. Lett.* **2012**, *3*, 503−510.

(21) Fuller, F. D.; Pan, J.; Gelzinis, A.; Butkus, V.; Senlik, S. S.; Wilcox, D. E.; Yocum, C. F.; Valkunas, L.; Abramavicius, D.; Ogilvie, J. P. Vibronic coherence in oxygenic photosynthesis. *Nat. Chem.* **2014**, *6*, 706−711.

(22) Romero, E.; Augulis, R.; Novoderezhkin, V. I.; Ferretti, M.; Thieme, J.; Zigmantas, D.; van Grondelle, R. Quantum coherence in photosynthesis for efficient solar-energy conversion. *Nat. Phys.* **2014**, *10*, 676−682.

(23) Linnanto, J.; Korppi-Tommola, J. Quantum chemical simulation of excited states of chlorophylls, bacteriochlorophylls and their complexes. *Phys. Chem. Chem. Phys.* **2006**, *8*, 663−687.

(24) Dreuw, A.; Head-Gordon, M. Single-reference ab initio methods for the calculation of excited states of large molecules. *Chem. Rev.* **2005**, *105*, 4009−4037.

(25) König, C.; Neugebauer, J. Quantum chemical description of absorption properties and excited-state processes in photosynthetic systems. *ChemPhysChem* **2012**, *13*, 386−425.

(26) Sundholm, D. Density functional theory calculations of the visible spectrum of chlorophyll a. *Chem. Phys. Lett.* **1999**, *302*, 480−484.

(27) Sundholm, D. Comparison of the electronic excitation spectra of chlorophyll *a* and pheophytin *a* calculated at density functional theory level. *Chem. Phys. Lett.* **2000**, *317*, 545−552.

(28) Cai, Z. L.; Sendt, K.; Reimers, J. R. Failure of density-functional theory and time-dependent density-functional theory for large extended π systems. *J. Chem. Phys.* **2002**, *117*, 5543−5549.

(29) Dahlbom, M. G.; Reimers, J. R. Successes and failures of time-dependent density functional theory for the low-lying excited states of chlorophylls. *Mol. Phys.* **2005**, *103*, 1057−1065.

(30) Cai, Z. L.; Crossley, M. J.; Reimers, J. R.; Kobayashi, R.; Amos, R. D. Density functional theory for charge transfer: the nature of the N-bands of porphyrins and chlorophylls revealed through CAM-B3LYP, CASPT2, and SAC-CI calculations. *J. Phys. Chem. B* **2006**, *110*, 15624−15632.

(31) Milne, B. F.; Toker, Y.; Rubio, A.; Nielsen, S. B. Unraveling the intrinsic color of chlorophyll. *Angew. Chem., Int. Ed.* **2015**, *54*, 2170−2173.

(32) Stockett, M. H.; Musbat, L.; Kjær, C.; Houmøller, J.; Toker, Y.; Rubio, A.; Milne, B. F.; Brøndsted Nielsen, S. The Soret absorption band of isolated chlorophyll *a* and *b* tagged with quaternary ammonium ions. *Phys. Chem. Chem. Phys.* **2015**, *17*, 25793−25798.

(33) Preciado-Rivas, M. R.; Mowbray, D. J.; Lyon, K.; Larsen, A. H.; Milne, B. F. Optical excitations of chlorophyll *a* and *b* monomers and dimers. *J. Chem. Phys.* **2019**, *151*, 174102.

(34) Frankcombe, T. J. Explicit calculation of the excited electronic states of the photosystem II reaction centre. *Phys. Chem. Chem. Phys.* **2015**, *17*, 3295−3302.

(35) Parusel, A. B. J.; Grimme, S. Theoretical study of the excited states of chlorophyll *a* and pheophytin *a*. *J. Phys. Chem. B* **2000**, *104*, 5395−5398.

(36) Hasegawa, J.; Ozeki, Y.; Ohkawa, K.; Hada, M.; Nakatsuji, H. Theoretical study of the excited states of chlorin, bacteriochlorin, pheophytin *a*, and chlorophyll *a* by the SAC/SAC-CI method. *J. Phys. Chem. B* **1998**, *102*, 1320−1326.

(37) Winter, N. O. C.; Hättig, C. Scaled opposite-spin CC2 for ground and excited states with fourth order scaling computational costs. *J. Chem. Phys.* **2011**, *134*, 184101.

(38) Suomivuori, C. M.; Winter, N. O.; Hättig, C.; Sundholm, D.; Kaila, V. R. Exploring the light-capturing properties of photosynthetic chlorophyll clusters using large-scale correlated calculations. *J. Chem. Theory Comput.* **2016**, *12*, 2644−2651.

(39) Zhang, L.; Silva, D.-A.; Zhang, H.; Yue, A.; Yan, Y.; Huang, X. Dynamic protein conformations preferentially drive energy transfer along the active chain of the photosystem II reaction centre. *Nat. Commun.* **2014**, *5*, 4170.

(40) Müh, F.; Plöckinger, M.; Renger, T. Electrostatic asymmetry in the reaction center of photosystem II. *J. Phys. Chem. Lett.* **2017**, *8*, 850−858.

(41) Tamura, H.; Saito, K.; Ishikita, H. Acquirement of water-splitting ability and alteration of the charge-separation mechanism in photosynthetic reaction centers. *Proc. Natl. Acad. Sci. U.S.A.* **2020**, *117*, 16373−16382.

(42) Sirohiwal, A.; Neese, F.; Pantazis, D. A. Protein matrix control of reaction center excitation in photosystem II. *J. Am. Chem. Soc.* **2020**, *142*, 18174−18190.

(43) Tamura, H.; Saito, K.; Ishikita, H. The origin of unidirectional charge separation in photosynthetic reaction centers: nonadiabatic quantum dynamics of exciton and charge in pigment-protein complexes. *Chem. Sci.* **2021**, *12*, 8131−8140.

(44) Sirohiwal, A.; Berraud-Pache, R.; Neese, F.; Izsák, R.; Pantazis, D. A. Accurate computation of the absorption spectrum of chlorophyll a with pair natural orbital coupled cluster methods. *J. Phys. Chem. B* **2020**, *124*, 8761−8771.

(45) Sirohiwal, A.; Neese, F.; Pantazis, D. A. How can we predict accurate electrochromic shifts for biochromophores? A case study on the photosynthetic reaction center. *J. Chem. Theory Comput.* **2021**, *17*, 1858−1873.

(46) Cignoni, E.; Cupellini, L.; Mennucci, B. A fast method for electronic couplings in embedded multichromophoric systems. *J. Phys.: Condens. Matter* **2022**, *34*, 304004.

(47) Cignoni, E.; Cupellini, L.; Mennucci, B. Machine learning exciton Hamiltonians in light-harvesting complexes. *J. Chem. Theory Comput.* **2023**, *19*, 965−977.

(48) Anda, A.; Hansen, T.; De Vico, L. Multireference excitation energies for bacteriochlorophylls A within light harvesting system 2. *J. Chem. Theory Comput.* **2016**, *12*, 1305−1313.

(49) De Vico, L.; Anda, A.; Osipov, V. A.; Madsen, A. Ø.; Hansen, T. Macrocycle ring deformation as the secondary design principle for light-harvesting complexes. *Proc. Natl. Acad. Sci. U.S.A.* **2018**, *115*, E9051−E9057.

(50) Umena, Y.; Kawakami, K.; Shen, J. R.; Kamiya, N. Crystal structure of oxygen-evolving photosystem II at a resolution of 1.9 Å. *Nature* **2011**, *473*, 55−60.

(51) The relative ground state energy of P_{D2} is 460 meV, or ≈18 k_BT, where 1 $k_BT \approx 8.617333262 \times 10^{-5}$ eV/K × 293.15 K ≈ 26 meV.[64]

(52) Gelzinis, A.; Valkunas, L.; Fuller, F. D.; Ogilvie, J. P.; Mukamel, S.; Abramavicius, D. Tight-binding model of the photosystem II reaction center: application to two-dimensional electronic spectroscopy. *New J. Phys.* **2013**, *15*, 075013.

(53) Shibata, Y.; Nishi, S.; Kawakami, K.; Shen, J.-R.; Renger, T. Photosystem II does not possess a simple excitation energy funnel: time-resolved fluorescence spectroscopy meets theory. *J. Am. Chem. Soc.* **2013**, *135*, 6903−6914.

(54) Novoderezhkin, V. I.; Romero, E.; Dekker, J. P.; van Grondelle, R. Multiple charge-separation pathways in photosystem II: modeling of transient absorption kinetics. *ChemPhysChem* **2011**, *12*, 681−688.

(55) Novoderezhkin, V. I.; Dekker, J. P.; van Grondelle, R. Mixing of exciton and charge-transfer states in photosystem II reaction centers: modeling of Stark spectra with modified Redfield theory. *Biophys. J.* **2007**, *93*, 1293−1311.

(56) Raszewski, G.; Saenger, W.; Renger, T. Theory of optical spectra of photosystem II reaction centers: location of the triplet state and the identity of the primary electron donor. *Biophys. J.* **2005**, *88*, 986−998.

(57) Novoderezhkin, V. I.; Palacios, M. A.; van Amerongen, H.; van Grondelle, R. Excitation dynamics in the LHCII complex of higher plants: modeling based on the 2.72 Å crystal structure. *J. Phys. Chem. B* **2005**, *109*, 10493−10504.

(58) Renger, T.; Marcus, R. A. On the relation of protein dynamics and exciton relaxation in pigment-protein complexes: an estimation of the spectral density and a theory for the calculation of optical spectra. *J. Chem. Phys.* **2002**, *116*, 9997−10019.

(59) Jankowiak, R.; Hayes, J. M.; Small, G. J. An excitonic pentamer model for the core Q_y states of the isolated photosystem II reaction center. *J. Phys. Chem. B* **2002**, *106*, 8803−8814.

(60) Prokhorenko, V. I.; Holzwarth, A. R. Primary processes and structure of the photosystem II reaction center: a photon echo study. *J. Phys. Chem. B* **2000**, *104*, 11563−11578.

(61) Durrant, J. R.; Klug, D. R.; Kwa, S. L.; van Grondelle, R.; Porter, G.; Dekker, J. P. A multimer model for P680, the primary electron donor of photosystem II. *Proc. Natl. Acad. Sci.* **1995**, *92*, 4798−4802.

(62) Abramavicius, D.; Mukamel, S. Energy-transfer and charge-separation pathways in the reaction center of photosystem II revealed by coherent two-dimensional optical spectroscopy. *J. Chem. Phys.* **2010**, *133*, 184501.

(63) Acharya, K.; Neupane, B.; Zazubovich, V.; Sayre, R. T.; Picorel, R.; Seibert, M.; Jankowiak, R. Site energies of active and inactive pheophytins in the reaction center of photosystem II from *Chlamydomonas reinhardtii*. *J. Phys. Chem. B* **2012**, *116*, 3890−3899.

(64) Newell, D. B.; Cabiati, F.; Fischer, J.; Fujii, K.; Karshenboim, S. G.; Margolis, H. S.; de Mirandés, E.; Mohr, P. J.; Nez, F.; Pachucki, K.; Quinn, T. J.; Taylor, B. N.; Wang, M.; Wood, B. M.; Zhang, Z. The CODATA 2017 values of *h*, *e*, *k*, and N_A for the revision of the SI. *Metrologia* **2018**, *55*, L13−L16.

(65) Cardoso Ramos, F.; Nottoli, M.; Cupellini, L.; Mennucci, B. The molecular mechanisms of light adaption in light-harvesting complexes of purple bacteria revealed by a multiscale modeling. *Chem. Sci.* **2019**, *10*, 9650−9662.

(66) Schreiber, M.; Silva-Junior, M. R.; Sauer, S. P. A.; Thiel, W. Benchmarks for electronically excited states: CASPT2, CC2, CCSD, and CC3. *J. Chem. Phys.* **2008**, *128*, 134110.

(67) Send, R.; Kaila, V. R. I.; Sundholm, D. Benchmarking the approximate second-order coupled-cluster method on biochromophores. *J. Chem. Theory Comput.* **2011**, *7*, 2473−2484.

(68) Sarkar, R.; Loos, P.-F.; Boggio-Pasqua, M.; Jacquemin, D. Assessing the performances of CASPT2 and NEVPT2 for vertical excitation energies. *J. Chem. Theory Comput.* **2022**, *18*, 2418−2436.

(69) Zobel, J. P.; Nogueira, J. J.; González, L. The IPEA dilemma in CASPT2. *Chem. Sci.* **2017**, *8*, 1482−1499.

(70) Roos, B. O.; Taylor, P. R.; Sigbahn, P. E. A complete active space SCF method (CASSCF) using a density matrix formulated super-CI approach. *Chem. Phys.* **1980**, *48*, 157−173.

(71) Roos, B. O.; Lindh, R.; Malmqvist, P. Å.; Veryazov, V.; Widmark, P. O. Main group atoms and dimers studied with a new relativistic ANO basis set. *J. Phys. Chem. A* **2004**, *108*, 2851−2858.

(72) Malmqvist, P. Å.; Pierloot, K.; Shahi, A. R. M.; Cramer, C. J.; Gagliardi, L. The restricted active space followed by second-order perturbation theory method: theory and application to the study of CuO_2 and Cu_2O_2 systems. *J. Chem. Phys.* **2008**, *128*, 204109.

(73) Sauri, V.; Serrano-Andrés, L.; Shahi, A. R. M.; Gagliardi, L.; Vancoillie, S.; Pierloot, K. Multiconfigurational second-order perturbation theory restricted active space (RASPT2) method for electronic excited states: a benchmark study. *J. Chem. Theory Comput.* **2011**, *7*, 153−168.

(74) Forsberg, N.; Malmqvist, P. Å. Multiconfiguration perturbation theory with imaginary level shift. *Chem. Phys. Lett.* **1997**, *274*, 196−204.

(75) Ghigo, G.; Roos, B. O.; Malmqvist, P. Å. A modified definition of the zeroth-order Hamiltonian in multiconfigurational perturbation theory (CASPT2). *Chem. Phys. Lett.* **2004**, *396*, 142−149.

(76) Aquilante, F.; Autschbach, J.; Baiardi, A.; Battaglia, S.; Borin, V. A.; Chibotaru, L. F.; Conti, I.; De Vico, L.; Delcey, M.; Fdez. Galván, I.; et al. Modern quantum chemistry with [open] Molcas. *J. Chem. Phys.* **2020**, *152*, 214117.

(77) Stewart, J. J. Optimization of parameters for semiempirical methods V: modification of NDDO approximations and application to 70 elements. *J. Mol. Model.* **2007**, *13*, 1173−1213.

(78) Frisch, M. J.; et al. *Gaussian 16*, Revision B.01, 2016.

(79) Aquilante, F.; Autschbach, J.; Carlson, R. K.; Chibotaru, L. F.; Delcey, M. G.; De Vico, L.; Fdez. Galván, I.; Ferré, N.; Frutos, L. M.; Gagliardi, L.; et al. Molcas 8: new capabilities for multiconfigurational quantum chemical calculations across the periodic table. *J. Comput. Chem.* **2016**, *37*, 506−541.